



Article

Synthesis and Properties of Cefixime Core–Shell Magnetic Nano-Molecularly Imprinted Materials

Li Zhang ¹, Hongbo Mo ², Chuan Wang ², Xiaofeng Li ², Shuai Jiang ², Weigang Fan ^{1,*}  and Yagang Zhang ³ 

¹ College of Chemistry and Chemical Engineering, Xinjiang Normal University, Urumqi 830054, China; 15099091024@163.com

² Chongqing Academy of Metrology and Quality Inspection, Chongqing 401123, China

³ School of Materials and Energy, University of Electronic Science and Technology, Chengdu 611731, China; ygzhang@uestc.edu.cn

* Correspondence: fwg19760123@xjnu.edu.cn

Abstract: Novel core–shell magnetic molecularly imprinted polymers (MMIPs) were synthesized using the sol–gel method for the adsorption of cefixime (CFX). Fe₃O₄@SiO₂ is the core, and molecularly imprinted polymers (MIPs) are the shell, which can selectively interact with CFX. The preparation conditions, adsorption kinetics, adsorption isotherms, selective adsorption ability, and reutilization performance of the MMIPs were investigated. The adsorption capacity of MMIPs for CFX was 111.38 mg/g, which was about 3.5 times that of MNIPs. The adsorption equilibrium time was 180 min. The dynamic adsorption experiments showed that the adsorption process of MMIPs to CFX conformed to the pseudo-second-order model. Through static adsorption study, the Scatchard analysis showed that MMIPs had two types of binding sites—the high-affinity binding sites and the low-affinity binding sites—while the Langmuir model fit the adsorption isotherms well ($R^2 = 0.9962$). Cefepime and ceftiofur were selected as the structural analogs of CFX for selective adsorption studies; the adsorption of CFX by MMIPs was higher than that of other structural analogs; and the imprinting factors of CFX, cefepime, and ceftiofur were 3.5, 1.7, and 1.4, respectively. Furthermore, the MMIPs also showed excellent reusable performance.

Keywords: magnetic; molecular imprinting polymers; cefixime; core–shell structure; adsorption



Citation: Zhang, L.; Mo, H.; Wang, C.; Li, X.; Jiang, S.; Fan, W.; Zhang, Y. Synthesis and Properties of Cefixime Core–Shell Magnetic Nano-Molecularly Imprinted Materials. *Polymers* **2023**, *15*, 4464. <https://doi.org/10.3390/polym15224464>

Academic Editors: Arunas Ramanavicius and Vilma Ratautaite

Received: 12 October 2023

Revised: 12 November 2023

Accepted: 14 November 2023

Published: 20 November 2023



Copyright: © 2023 by the authors. Licensee MDPI, Basel, Switzerland. This article is an open access article distributed under the terms and conditions of the Creative Commons Attribution (CC BY) license (<https://creativecommons.org/licenses/by/4.0/>).

1. Introduction

Cefixime (CFX), an important β -lactam ring antibiotic, is mainly used to treat throat infections, gonorrhea, and pneumonia [1,2]. Advantages such as strong antibacterial activity and good efficacy have enabled the wide use of CFX in the treatment of diseases in humans, poultry, and aquaculture [3,4]. However, its frequent use has raised concerns over harm to both the environment and human health. In the production process of CFX, the separation, extraction, purification, and other processes will produce high-concentration organic wastewater. CFX has been detected in the water and soil of many countries and regions; for example, high concentrations of CFX were found in hospital wastewater in Bangladesh [5], which is difficult to treat due to its strong polarity and biological enrichment [6]. At present, the removal technologies of CFX in the environment mainly include physical separation, biodegradation, chemical oxidation, etc. [7–9]. Vajihe Hasanzadeh et al. used metal hydroxide to activate jujube fruit residue at high temperature, which adsorbed CFX based on physical separation [10]. Physical separation is complex, requires high temperature, and has poor specificity for pollutants. Abotaleb Bay et al. developed a biofilm reactor for treating CFX in wastewater. The degradation rate could reach 70.9% at 92 mg/L, but the degradation efficiency was reduced to 34.8% at 122 mg/L [11]. In the process of biodegradation, there are disadvantages; for example, toxic substances may be produced, and rigorous temperature conditions are required. The operation cost of chemical oxidation is high, the operation is complicated, and toxic products may still be produced

after degradation. For example, Hasani et al. degraded CFX in water via the ultrasonic and electric Fenton method, but the cost was high, the operation was complicated, and toxic products might still have been produced after degradation [12]. Therefore, it is necessary to design a low-cost material, which can identify CFX in complex systems.

MIPs are synthetic materials with a specific selection of target molecules [13], which, owing to their imprinted site, are complementary to the target molecules in shape and size [14,15], vividly described as artificially synthesized tailor-made polymers [16,17]. MIPs benefit from excellent properties, such as prominent selectivity, strong anti-interference ability, and convenient synthesis [18–20]. They have application opportunities in solid phase extraction, controlled drug release, sensors, and catalysis [21,22]. However, the use of traditional MIPs includes obstacles related to their low binding capacity and mass transfer [23–25]. By designing the molecular recognition sites on the surface of imprinted materials, the surface molecular imprinting technology improves the mass transfer between the recognition sites and target molecules, facilitates the elution and recombination of template molecules, improves the recognition efficiency and binding speed, and avoids the disadvantages of traditional methods.

The molecular imprinting technique of graft on the surface of a carrier has been extensively studied. The commonly used carriers include SiO_2 , TiO_2 , Al_2O_3 , magnetic nanomaterials, etc. Shichao Ding et al. designed and synthesized peptide-imprinted mesoporous silica using a combination of the sol–gel method and molecular imprinting technology to specifically identify an immunostimulating hexapeptide from human casein; the adsorption capacity was 60.5 mg/g, and the imprinting factor was 4.51 [26]. In terms of the application effect, magnetic nanoparticles have received attention due to their good dispersion, controllability, small size, and excellent superparamagnetism [27,28]. MMIPs can not only specifically adsorb target molecules in a complex environment, but they can also be quickly separated by an external magnetic field, thus avoiding steps such as centrifugation, resulting in low cost, mild conditions, reducing material waste, and improving work efficiency [29,30]. Fatemeh Mirzapour et al. prepared the MMIPs of dextromethorphan via precipitation polymerization using $\text{Fe}_3\text{O}_4@ \text{SiO}_2\text{-C}=\text{C}$ as the carrier and applied them to highly selective solid phase extraction; the recovery was 92–97%, and the adsorption capacity was 114.8 mg/g [31]. Chaoren Yan et al. used $\text{Fe}_3\text{O}_4@ \text{SiO}_2$ as the carrier and developed a combination of epigallocatechin-3-gallate (EGCG), imprinting technology, and magnetic nanoparticles to obtain a somewhat promising nanomaterial (MINs@EGCG) for amyloid inhibition, drug carrier, and facile separation triple functions; the cleansing efficiency was up to 80% [32]. Shikha Bhogal et al. prepared MMIPs for phthalate adsorption via surface imprinting using $\text{Fe}_3\text{O}_4@ \text{SiO}_2$ as a carrier; the recovery was 88.53–121.57%, with LOD ranging from 0.01 to 0.03 ng/mL [33]. Ziyang Lu et al. prepared a magnetic imprinted PEDOT/CdS nanoreactor for the adsorption and degradation of danofloxacin mesylate through the microwave-assisted surface imprinting technique, with a degradation rate of 84%; the adsorption capacity was 1.41 mg/g [34]. Mir Muhammad Gaho et al. prepared the MMIPs for norfloxacin adsorption through radical polymerization using oleic-coated Fe_3O_4 as the carrier, and the maximum adsorption capacity was 42.34 mg/g at 35 °C [35]. Ziyang Li et al. prepared the MMIPs for sulfamethoxazole using Fe-Mn impregnated peanut shell biochar as a functional monomer by using surface molecular imprinting technology, with a maximum adsorption capacity of 25.65 mg/g and an imprinting factor of 1.34 [36]. Notably, there are few reports on the adsorption of CFX on MMIPs, which is where our work was focused.

In this work, the sol–gel method was introduced to imprint molecules into the inorganic network structures to form a rigid structure. Compared with precipitation polymerization, radical polymerization, and other methods, this method is simple in operation, easy to control, and low cost [31,37–39]. $\text{Fe}_3\text{O}_4@ \text{SiO}_2$ was the core, and MIPs were used as the shell; silica was used as the intermediate carrier to connect the magnetic particles and the organic layer. CFX was used as the template, 3-aminopropyltriethoxysilane (APTES) as a functional monomer, and tetraethoxysilane (TEOS) as a crosslinker to be imprinted on

the surface of Fe₃O₄@SiO₂ with the sol–gel method. Thus, MMIPs with core–shell were prepared and showed high selectivity toward CFX.

2. Experimental Section

2.1. Materials

CFX, TEOS, cefepime, ceftiofur, and APTES were purchased from Aladdin Reagent Co., Ltd. (Shanghai, China). Crystalline sodium acetate, ethylene glycol, and polyethylene glycol 6000 (PEG) were purchased from Tianjin Zhiyuan Chemical Reagent (Tianjin, China). NH₃·H₂O (25%), methanol, ethanol, and acetic acid were purchased from Shanghai Chemical Reagent Co. (Shanghai, China).

2.2. Characterization

Infrared spectra were analyzed using Fourier transform infrared spectroscopy (FTIR; Tensor 27, Bruker, Billerica, MA, USA). The crystalline structures of the MMIPs were characterized via X-ray diffraction (XRD; D8, Bruker, Salbuluken, Germany). The magnetic properties were characterized through vibrating sample magnetometry (VSM; 7404, Lake Shore Company, Columbus, OH, USA). Morphological analysis was characterized through scanning electron microscopy (SEM; Sigma300, Zeiss, Berlin, Germany). Finally, the morphology of the MMIPs was characterized via transmission electron microscopy (TEM; JSM-7610FPlus, JEOL, Tokyo, Japan).

2.3. Preparation of MMIPs and Magnetic Non-Molecularly Imprinted Polymers (MNIPs)

2.3.1. Preparation and Modification of Fe₃O₄

Fe₃O₄ was synthesized using the solvent-thermal method [40]. First, 2.025 g FeCl₃·6H₂O was dissolved in 60 mL ethylene glycol; then, 5.50 g NaAc and 1.50 g PEG were added, and the mixture was stirred magnetically. Finally, the mixture was sealed in the reactor at 190 °C for 8 h. The unreacted material was washed alternately with ultrapure water and ethanol and dried under a vacuum. The Fe₃O₄ nanoparticles were modified with SiO₂ based on the hydrolysis of TEOS, according to the literature [41]. Subsequently, 0.2 g Fe₃O₄ was dispersed in a 125 mL solution of ethanol and ultrapure water (4:1, *v/v*), after which 1.8 mL NH₃·H₂O and 0.6 mL TEOS were added; the material was dried at 60 °C for 10 h in a vacuum to obtain Fe₃O₄@SiO₂.

2.3.2. Synthesis of MMIPs and MNIPs

Amounts of 0.135 g CFX, 0.420 mL APTES, and 30 mL methanol were mixed and stirred; then, amounts of 2.67 mL TEOS, 0.20 g Fe₃O₄@SiO₂, and 1 mL acetic acid (1 mol/L) were added, and the mixture was stirred for 10 h. The mixture was then separated with magnets, washed repeatedly, and dried. A mixture of methanol/acetic acid (9:1, *v/v*) was used to elute CFX from the MMIPs until there was no UV-Vis adsorption at 288 nm. Then, the MMIPs were vacuum-dried at 60 °C for 10 h. The MNIPs were prepared without CFX but using the same protocol.

2.4. Binding Experiments

2.4.1. Static Adsorption

An amount of 5 mg of MMIPs or MNIPs was added to a 10 mL CFX–methanol solution of 10–200 mg/L, which was shaken for 180 min; magnets were used for separation, and the absorbance of the supernatant was measured at 288 nm with UV-Vis. The adsorption capacity *Q* (mg/g) was calculated according to the following formula:

$$Q = (C_0 - C_e)V/m \quad (1)$$

where *C*₀ (mg/L) is the initial concentration of the CFX solution; *C*_{*e*} (mg/L) is the equilibrium concentration of CFX; *V* (L) is the total volume; and *m* (g) is the weight of the MMIPs or MNIPs.

2.4.2. Adsorption Kinetics

MMIPs or MNIPs (5 mg) were added to a 10 mL CFX–methanol solution of 200 mg/L and shaken at 25 °C for different times (30–240 min), and magnets were used for separation. The absorbance of CFX was measured using UV-Vis.

2.5. Selectivity

The selectivity of MMIPs was assessed using cefepime and ceftiofur as the structural analogs of CFX. MMIPs or MNIPs (5 mg) were added to 200 mg/L of methanol solution containing each compound. We used the imprinted factor (*IF*) to assess the selectivity of MMIPs, which is defined as

$$IF = Q_{MMIPs} / Q_{MNIPs} \quad (2)$$

where Q_{MMIPs} and Q_{MNIPs} are the binding capacities of MMIPs and MNIPs, respectively.

2.6. Reusability

To evaluate the repetitive utilization rate, 5 mg of MMIPs was added to a 10 mL CFX–methanol solution of 200 mg/L and oscillated for 180 min, followed by magnetic field separation. The CFX in the MMIPs was washed with methanol/acetic acid (9:1, *v/v*), dried in a vacuum, and prepared for the next adsorption of CFX. The process was repeated five times.

3. Results and Discussion

3.1. Preparation of MMIPs and MNIPs

Fe₃O₄ nanoparticles exhibit a strong aggregation tendency and are easily oxidized in air [42,43]; therefore, we used Fe₃O₄ with silica modification. The synthesis process of MMIPs was as follows: (1) silica shell deposition on the surface of Fe₃O₄, (2) MIPs layer imprinting on Fe₃O₄@SiO₂, and (3) removal of template molecules. The MIPs were imprinted on Fe₃O₄@SiO₂ through the interaction of CFX, APTES, and TEOS. The carboxyl group of CFX interacts with the amino group of APTES to form a hydrogen bond; after eluting, the specific recognition sites for CFX are formed, ensuring that MMIPs can specifically recognize CFX. A schematic of the synthesis of CFX–MMIPs is shown in Figure 1.

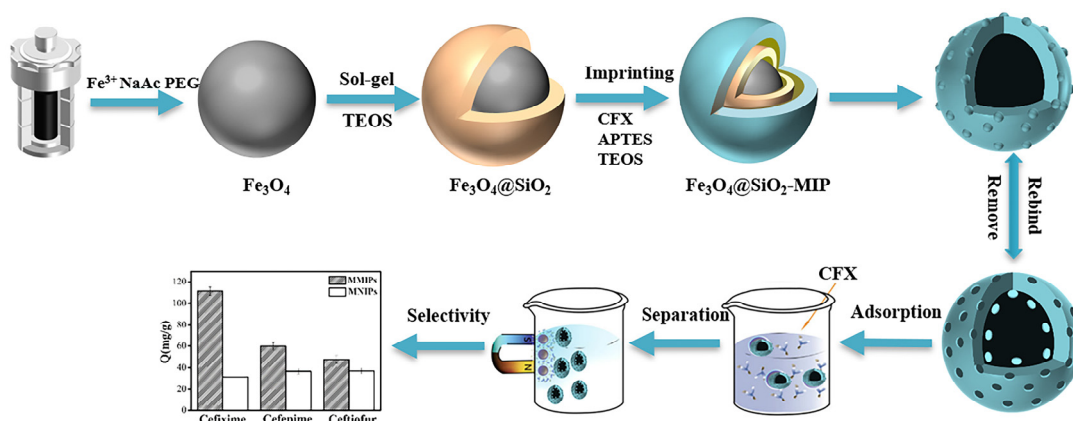


Figure 1. Schematic of the synthesis of CFX–MMIPs.

3.2. Optimization of the Synthesis Conditions

3.2.1. The Ratio of the Reactants

The ratio of the template molecule and crosslinker affects the property of MMIPs [44], including the stability of the recognized site and the mechanical strength of the polymer. The crosslinker binds the template molecule to the functional monomer, and an appropriate amount of crosslinker facilitates the formation of a rigid cavity for the adsorption of the target molecule. The amount of crosslinker is important; too little will render the synthesized polymer too soft to form stable affinity sites, while too much will cause an

excessively high degree of crosslinking [45]. The excessive crosslinker will cover the recognition cavity and make it difficult for the elution of the template molecule, causing mass transfer resistance and adversely affecting the adsorption [46]. Therefore, to obtain better selective MMIPs, the ratio of the reactants should be carefully considered.

As shown in Figure 2a, the adsorption capacity first increased and then decreased with an increase in the TEOS ratio. When the ratio was 1:6:40, the adsorption capacity reached a maximum; when the ratio exceeded 1:6:40, the adsorption capacity was reduced, which could have resulted from excessive TEOS hindering the elution of the template molecule and blocking CFX from the recognition site. When the ratio was less than 1:6:40, the MMIPs exhibited poor performance in the adsorption capacity. Thus, for the rigid construction of MMIPs with a high binding capacity, the optimal molar ratio of CFX, APTES, and TEOS was 1:6:40.

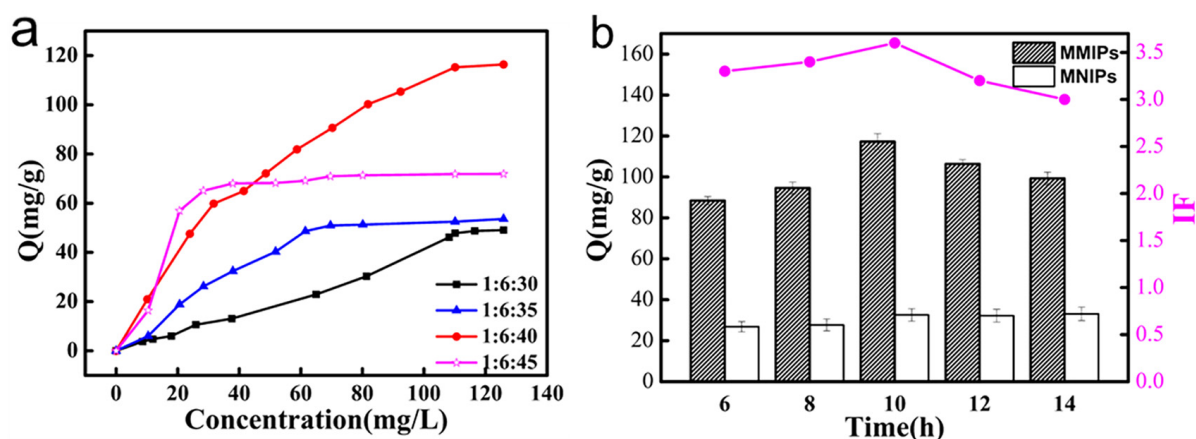


Figure 2. Effect of the crosslinker on the binding property of MMIPs: (a) The adsorption capacity of MMIPs and MNIPs at different polymerization times (b).

3.2.2. Influence of Polymerization Time

The polymerization time of the MMIPs significantly affected the adsorption capacity of CFX, and polymerization times of 6, 8, 10, 12, and 14 h were selected for investigation (Figure 2b). A polymerization time of less than 10 h resulted in a low adsorption capacity, possibly due to fewer imprinting sites. At a polymerization time of 10 h, the adsorption capacity reached its maximum. However, a polymerization time longer than 10 h resulted in a decreased adsorption capacity, possibly due to CFX having difficulty reaching the imprinted sites. Therefore, the optimum polymerization time was 10 h.

3.3. Characteristics of MMIPs and MNIPs

The FTIR spectra of Fe_3O_4 , $\text{Fe}_3\text{O}_4@\text{SiO}_2$, MMIPs, and MNIPs (Figure 3) show a peak at 577 cm^{-1} , which is the typical band of Fe_3O_4 [47] (Figure 3a). The new peak at 1082 cm^{-1} in the spectrum of $\text{Fe}_3\text{O}_4@\text{SiO}_2$ is attributed to Si–O–Si, and the peaks at 954 cm^{-1} and 800 cm^{-1} represent the vibration absorption of the Si–O bond in Si–OH and the bending vibration absorption peak of Si–O–Si, indicating the successful synthesis of $\text{Fe}_3\text{O}_4@\text{SiO}_2$ (Figure 3b). Meanwhile, the characteristic peaks of the N–H bond at 1543 cm^{-1} , Si–O–Si and Si–O–H bonds at 1082 cm^{-1} , and C–H stretching at 2930 cm^{-1} are the results of the imprinted layer being successfully bonded to the surface of $\text{Fe}_3\text{O}_4@\text{SiO}_2$ by reacting with CFX, APTES, and TEOS [48]. Peaks at 1720 cm^{-1} (C=O) and 3226 cm^{-1} (O–H) were observed, indicating the presence of carboxyl groups in the MMIPs [49]. The characteristic absorption peaks of the MMIPs and MNIPs were not significantly different (Figure 3c,d), indicating that the addition of template molecules did not change the main functional groups of the polymer.

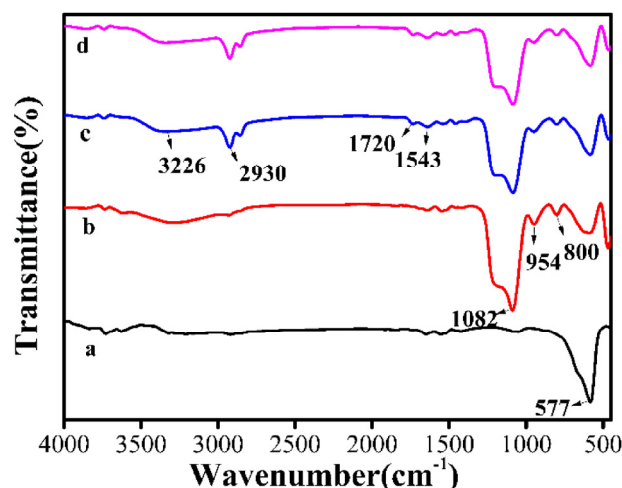


Figure 3. FTIR spectra of Fe_3O_4 (a), $\text{Fe}_3\text{O}_4@\text{SiO}_2$ (b), MMIPs (c), and MNIPs (d).

Figure 4 depicts the XRD pattern of Fe_3O_4 , $\text{Fe}_3\text{O}_4@\text{SiO}_2$, and MMIPs. The characteristic XRD absorption peaks of Fe_3O_4 appeared at $2\theta = 30.38^\circ$, 35.58° , 43.14° , 53.48° , 57.08° , and 62.66° , corresponding to the stereoscopic crystal planes (220), (311), (400), (422), (511), and (440) of Fe_3O_4 , respectively. This is consistent with the JCPDS-International Centre (JCPDS Card: 19-629) and proves that the prepared product was Fe_3O_4 . When $2\theta = 22^\circ$, there is a wider diffraction peak corresponding to the amorphous SiO_2 in $\text{Fe}_3\text{O}_4@\text{SiO}_2$ (Figure 4b). The weakening of the peak at $2\theta = 22^\circ$ was due to an imprinting layer on the $\text{Fe}_3\text{O}_4@\text{SiO}_2$ surface (Figure 4c). The distinguishable characteristic diffraction peaks of Fe_3O_4 were observed for the three samples, indicating that the crystal structure of Fe_3O_4 remained unchanged during the imprinting process and was incorporated into all the samples.

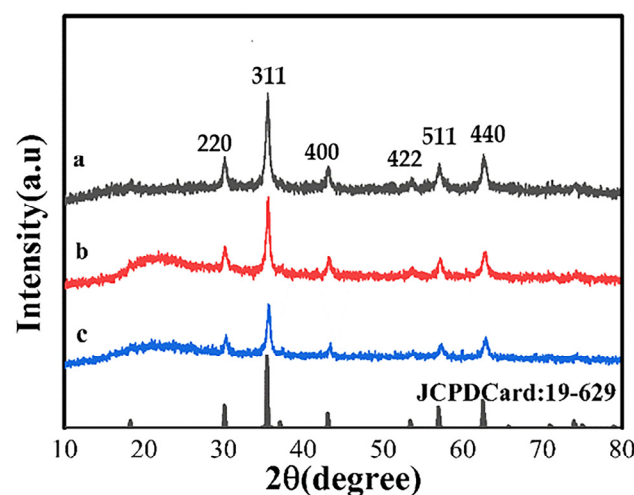


Figure 4. XRD pattern of Fe_3O_4 (a), $\text{Fe}_3\text{O}_4@\text{SiO}_2$ (b), and MMIPs (c).

The magnetic properties of synthetic materials were analyzed using VSM. As illustrated (Figure 5), the synthetic materials crossed the zero point, showing superparamagnetic properties with almost no coercivity or remanence, indicating that the particles could be dispersed in a short time and exhibited a strong response to the magnetic field. The saturation magnetization (M_s) values of Fe_3O_4 , $\text{Fe}_3\text{O}_4@\text{SiO}_2$, and MMIPs were 87.2 emu/g, 61.0 emu/g, and 32.2 emu/g, respectively. The M_s of MMIPs showed a slight decrease compared to Fe_3O_4 , which was attributed to the shielding effect of the Fe_3O_4 surface parcel Si coating and the molecularly imprinted layer. However, the MMIPs were still magnetic enough to meet the requirements of an effective magnetic carrier and could be separated

by external magnets. As shown in the inset of Figure 5, the MMIPs were attracted to the bottle wall within 20 s, and the dispersed liquid became transparent, further verifying the successful synthesis and excellent magnetic properties of MMIPs.

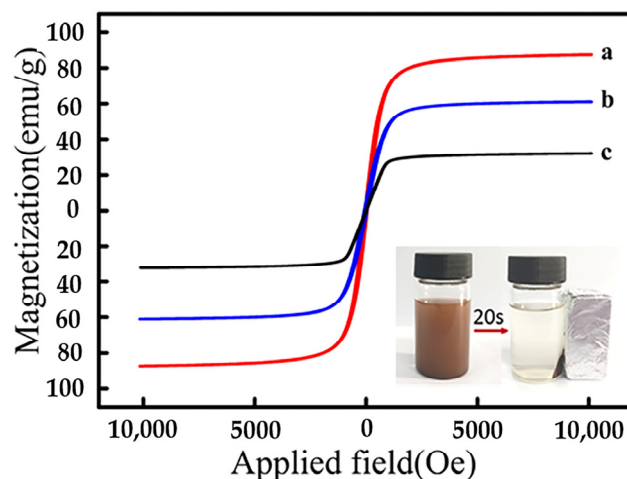


Figure 5. Magnetic hysteresis loop of Fe_3O_4 (a), $\text{Fe}_3\text{O}_4@\text{SiO}_2$ (b), MMIPs (c), and the inserted figure depicts MMIPs dispersed in solution (left) and collected by an external magnet (right).

The synthetic materials were characterized by TEM, and the image of Fe_3O_4 (Figure 6a) shows a uniform size distribution with good dispersion and no obvious agglomeration. After silanization, the particle size changed significantly, corresponding to the approximately 50 nm layer of silica evenly coating the surface of Fe_3O_4 (Figure 6b), providing evidence that Fe_3O_4 was completely and uniformly coated by silica. After imprinting CFX as the template, the imprinting layer was observed to be approximately 60 nm (Figure 6c), which may have been caused by the combined reaction of organic compounds on the particle surface. These observations initially confirmed that the MMIPs were prepared.

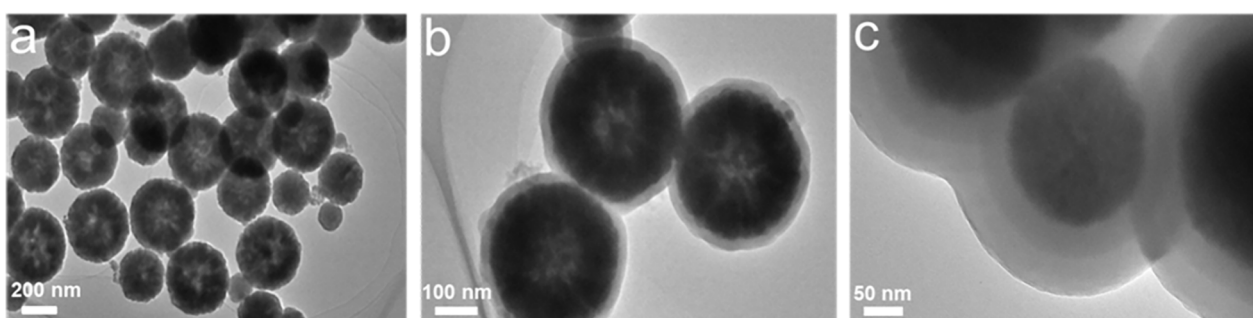


Figure 6. TEM of Fe_3O_4 (a), $\text{Fe}_3\text{O}_4@\text{SiO}_2$ (b), and MMIPs (c).

We used SEM to intuitively observe the surface morphology characteristics, and Figure 7 shows the morphological structures of MMIPs and MNIPs. The imprinted polymer surface became rough and uneven, indicating tiny “cavities” in the polymer surface and illustrating the deposition of the polymers over the surface of $\text{Fe}_3\text{O}_4@\text{SiO}_2$. The rough surface of the polymer, which improves the adsorption capacity and recognition ability of the template, resulted from the remaining imprinted cavities after template elution. The MMIPs and MNIPs exhibited surface differences, where the latter had a relatively smooth and flat surface. This further elucidated the differences in adsorption effects, as the MMIPs had cavities, which could specifically recognize CFX, and thus, better adsorption.

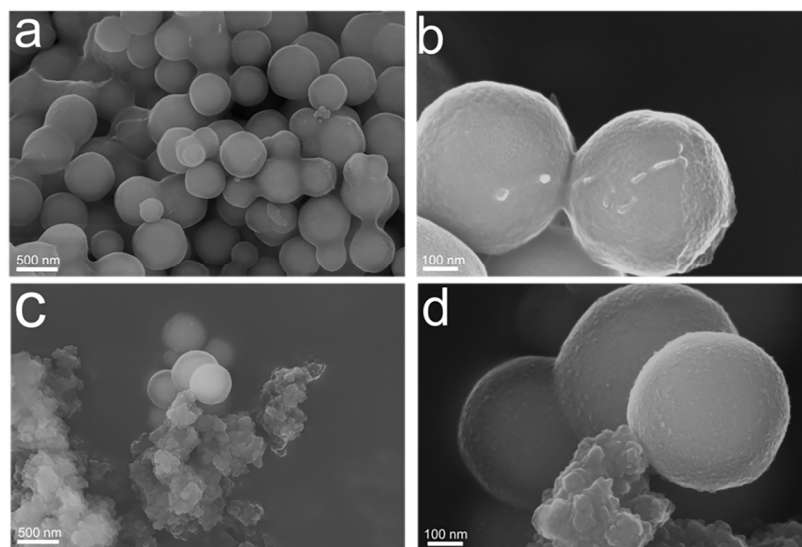


Figure 7. SEM of MMIPs (a,b) and MNIPs (c,d).

3.4. Adsorption Properties of MMIPs and MNIPs

3.4.1. Dynamic Adsorption

The adsorption kinetics of MMIPs and MNIPs were determined (Figure 8a), revealing that MMIPs could rapidly adsorb CFX in less than 150 min, after which the rate of adsorption capacity growth gradually decreased, finally reaching saturation after 180 min. Since there were imprinted sites on the surface of MMIPs at the initial stage of adsorption, CFX was rapidly adsorbed. After 180 min, an increasing number of binding sites were occupied, and the mass transfer of CFX in solution to the internal pores was subject to resistance. The adsorption capacity of MMIPs was approximately 3.52 times higher than MNIPs because CFX was not involved in the preparation of MNIPs; as such, there were no specific recognition holes or imprinting sites. The adsorption of CFX by MNIPs was mainly caused by non-specific adsorption of van der Waals force and other forces.

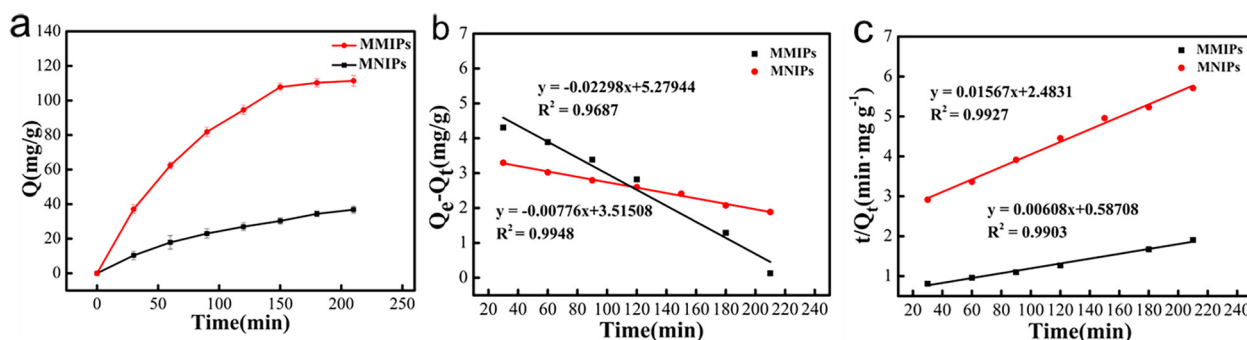


Figure 8. Kinetic adsorption curve of MMIPs and MNIPs (a): Fitting using a pseudo-first-order (b) and pseudo-second-order (c) kinetic model for the binding CFX.

To study the mass transfer mechanism of polymer-adsorbed CFX, the equilibrium data were fitted using the two models of pseudo-first-order and pseudo-second-order binding as follows [50]:

$$\ln(Q_e - Q_t) = \ln Q_e - k_1 t \tag{3}$$

$$\frac{t}{Q_t} = \frac{t}{Q_e} + \frac{1}{k_2 Q_e^2} \tag{4}$$

where Q_e is the adsorption equilibrium capacity of MMIPs or MNIPs, and Q_t is the adsorption capacity at time t ; t (min) is the adsorption time; and k_1 (min^{-1}) and k_2 ($\text{mg g}^{-1} \text{min}^{-1}$) are the pseudo-first-order and pseudo-second-order rate constants of adsorption, respectively.

The fitted data are shown in Table 1; the pseudo-second-order model (Figure 8c) was better than the pseudo-first-order model (Figure 8b). The adsorption process by MMIPs conformed to the pseudo-second-order model, and the adsorption process was controlled by chemisorption.

Table 1. Adsorption kinetic constants of pseudo-first-order and pseudo-second-order models for MMIPs and MNIPs.

Materials	$Q_{e,exp}$ (mg g^{-1})	Pseudo-First-Order Model			Pseudo-Second-Order Model		
		$Q_{e,cal}$ (mg g^{-1})	K_1 (min^{-1})	R^2	$Q_{e,cal}$ (mg g^{-1})	K_2 ($\text{mg g}^{-1} \text{min}^{-1}$)	R^2
MMIPs	111.38	196.25	0.0230	0.9687	164.47	0.0063	0.9903
MNIPs	36.15	27.52	0.0070	0.9948	64.10	0.0010	0.9927

3.4.2. Static Adsorption

The adsorption isotherms (at 25 °C) are shown in Figure 9a. At the same concentration, the adsorption capacity of MMIPs was higher than that of MNIPs, and the maximum adsorption capacity of MMIPs was 111.38 mg/g, which indicated that MMIPs had specific adsorption sites for CFX compared with MNIPs.

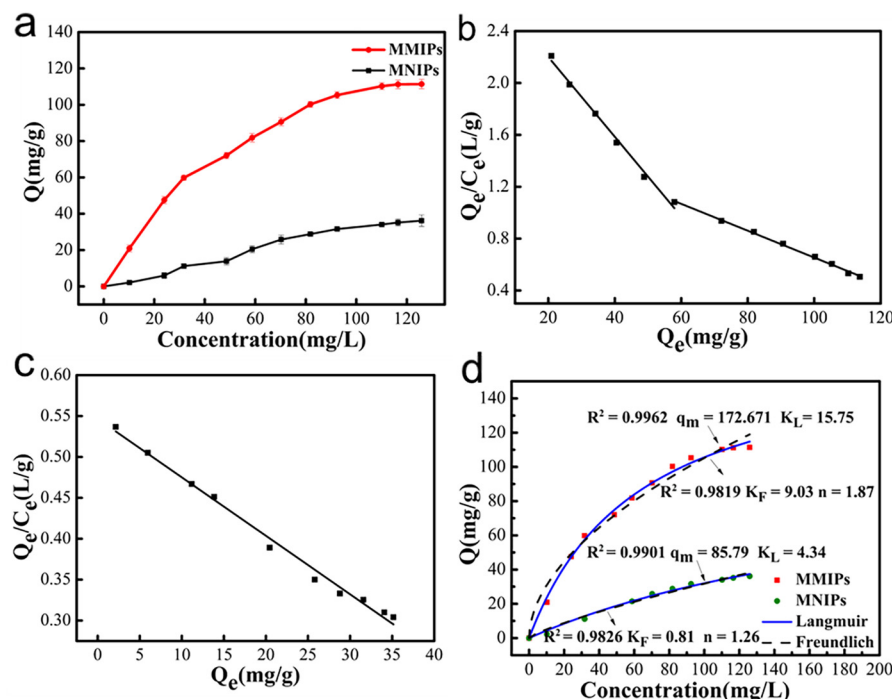


Figure 9. Adsorption isotherm of MMIPs and MNIPs (a); Scatchard plot analysis of CFX binding onto MMIPs (b) and MNIPs (c); Langmuir and Freundlich adsorption isotherms of CFX onto MMIPs and MNIPs (d).

To study the specific binding properties between MMIPs and CFX, Scatchard analysis was used to analyze the binding data. The results of the Scatchard analysis are shown in Table 2, and the Scatchard equation is as follows:

$$\frac{Q_e}{C_e} = \frac{Q_m}{K_d} - \frac{Q_e}{K_d} \tag{5}$$

where Q_e (mg/g) is the adsorption capacity of the MMIPs at equilibrium; Q_m (mg/g) is the maximum adsorption capacity; C_e (mg/L) is the concentration of the supernatant at equilibrium; and K_d (mg/L) is the equilibrium dissociation constant.

Table 2. Results of the Scatchard analysis.

Materials	Binding Site	Linear Equation	k_d (mg/L)	Q_{max} (mg/g)
MMIPs	Higher affinity site	$Q/C_e = -0.0307 Q + 2.815$ ($R^2 = 0.9914$)	32.542	91.604
		$Q/C_e = -0.0103 Q + 1.689$ ($R^2 = 0.9972$)	96.618	163.217
MNIPs	Lower affinity site	$Q/C_e = -0.0071 Q + 0.546$ ($R^2 = 0.9960$)	39.860	76.443

As shown in Figure 9b, there were two distinct linear sections, indicating that two types of binding sites with different binding properties existed on the surface of the MMIPs. This is because a variety of complexes with different stabilities can be formed between CFX and APTES, and different types of complexes form binding sites with different adsorption properties during polymerization. K_{d1} and Q_{max1} for the linear section on the left were calculated to be 32.542 mg/L and 91.6043 mg/g, respectively, and those for the linear section on the right were calculated to be 96.618 mg/L and 163.217 mg/g, respectively. Because $K_{d1} < K_{d2}$, the equation on the left corresponds to the high-affinity binding sites of MMIPs, while the equation on the right corresponds to the low-affinity binding sites of MMIPs. In contrast, the Scatchard fitted curve of the MNIPs (Figure 9c) shows only one straight line, which indicates that there was only one non-specific recognition site in the MNIPs.

The binding data were analyzed using the Langmuir and Freundlich isotherm models to assess the maximum adsorption capacities of MMIPs and MNIPs. The Langmuir isotherm model describes a monolayer adsorption process and assumes that adsorption occurs at specific and uniform adsorption points within the adsorbent [51].

The Freundlich model is suitable for multilayer adsorption [52]. The Freundlich and Langmuir equations are, respectively, expressed as follows [22]:

$$Q_e = K_F C_e^{1/n} \quad (6)$$

$$Q_e = \frac{Q_m K_L C_e}{1 + K_L C_e} \quad (7)$$

where Q_e and Q_m are the equilibrium and maximum adsorption amounts of MMIPs (mg/g), respectively; C_e is the equilibrium concentration of CFX (mg/L); K_L is the Langmuir model constant; and K_F and n are the Freundlich model constants (mg/L).

The correlation constants were calculated using the Freundlich and Langmuir models. The Langmuir isotherm was well fitted and could better describe the binding process (Figure 8d). It could therefore be inferred that the adsorption of CFX on MMIPs was monolayer adsorption.

3.5. Specificity

The adsorption selectivity of MMIPs for CFX was studied. Cefepime and ceftiofur were selected as the structural analogs of CFX (Figure 10). As shown in Figure 11, the adsorption of CFX by MMIPs was higher than that of the other structural analogs, indicating a high selectivity of MMIPs for CFX. For MNIPs, however, the adsorption of CFX and the other analogs was not significantly different. The IF values of CFX, cefepime, and ceftiofur were 3.5, 1.7, and 1.4, respectively.

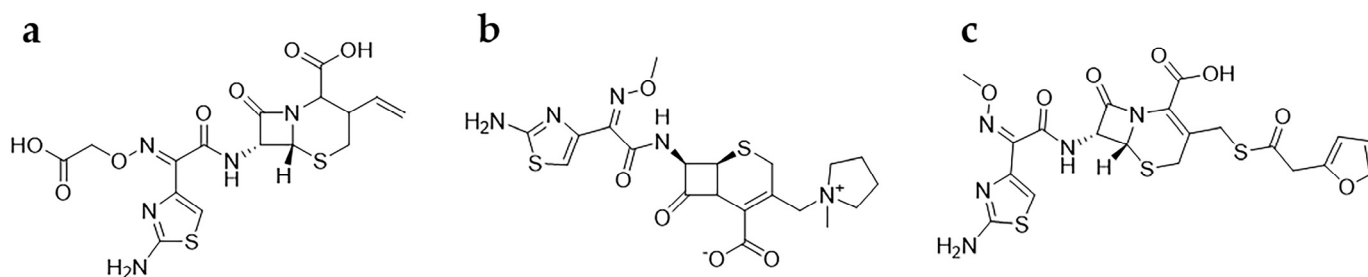


Figure 10. Structures of cefixime (a), cefepime (b), and ceftiofur (c).

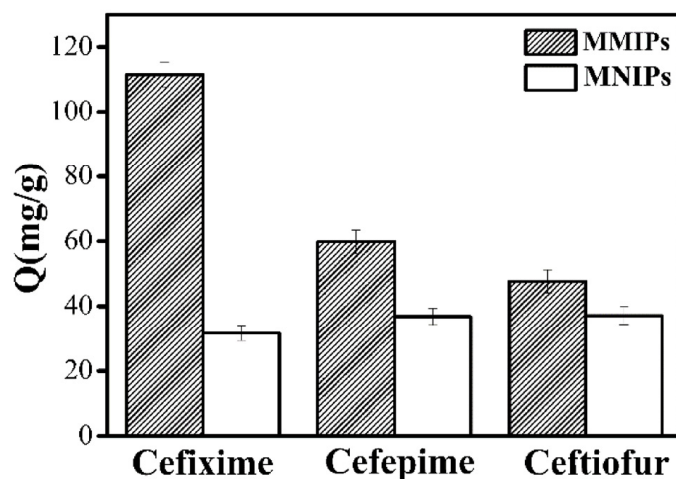


Figure 11. Adsorption capacities of CFX and its structural analogs.

3.6. Reusability

The reusability of MMIPs is important for economical, reliable, and sustainable applications. Thus, five adsorption–desorption cycles were investigated (Figure 12). The adsorption capacity of MMIPs decreased by 9.7% with repeated use. The decrease may have been due to the destruction of imprinting recognition sites through multiple adsorption–desorption cycles, showing that the adsorption capacity remained high after multiple applications and indicating that the MMIPs had outstanding regeneration. Therefore, the MMIPs exhibited strong potential for practical applications.

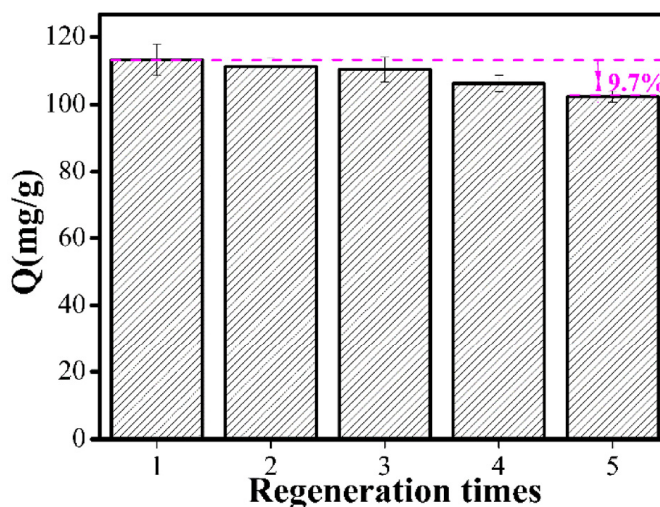


Figure 12. Regeneration properties of MMIPs.

4. Conclusions

Using CFX as a template molecule, APTES as a functional monomer, and TEOS as a crosslinker, a surface-molecule-imprinted polymer with specific adsorption of CFX was synthesized on the surface of Fe₃O₄@SiO₂ via surface imprinting technology, which could achieve rapid separation under the external magnetic field. The adsorption performance of MMIPs was evaluated through adsorption kinetics, adsorption isotherm, and reusability. The results showed that MMIPs could reach the adsorption equilibrium within 180 min, with a good imprinting effect and selectivity (imprinting factor 3.5), high adsorption capacity (111.38 mg/g), and excellent reuse performance (after five cycles of utilization, the adsorption capacity of cefixime could still be maintained at 90.3%). The synthesized molecularly imprinted polymer can be used as a new adsorption material, with high selectivity and high adsorption capacity for cefixime.

Author Contributions: L.Z.: Investigation, Material preparation, Data curation, Formal analysis, Writing—original draft; H.M.: Validation, Conceptualization, Writing—review and editing; C.W.: Investigation, Data curation, Formal analysis; X.L.: Investigation, Data curation, Formal analysis; S.J.: Validation, Supervision, Conceptualization, Software; W.F.: Validation, Supervision, Conceptualization, Funding acquisition, Writing—review and editing; Y.Z.: Investigation, Conceptualization, Supervision. All authors have read and agreed to the published version of the manuscript.

Funding: This research was funded by the Natural Science Foundation of Xinjiang Uygur Autonomous Region (Grant No. 2022D01A210).

Institutional Review Board Statement: Not applicable.

Data Availability Statement: The data presented in this study are available on request from the corresponding author.

Conflicts of Interest: The authors declare no conflict of interest.

References

1. Masoudyfar, Z.; Elhami, S. Surface plasmon resonance of gold nanoparticles as a colorimetric sensor for indirect detection of Cefixime. *Spectrochim. Acta Part A* **2019**, *211*, 234–238. [[CrossRef](#)]
2. Karimian, N.; Gholivand, M.; Malekzadeh, G. Cefixime detection by a novel electrochemical sensor based on glassy carbon electrode modified with surface imprinted polymer/multiwall carbon nanotubes. *J. Electroanal. Chem.* **2016**, *771*, 64–72. [[CrossRef](#)]
3. Jaiswal, V.; Rastogi, R.B.; Kumar, D. Tribological investigations on β -lactam cephalosporin antibiotics as efficient ashless antiwear additives with low SAPS and their theoretical studies. *RSC Adv.* **2014**, *4*, 30500–30510.
4. Dubala, A.; Nagarajan, J.S.K.; Vimal, C.S.; George, R. Simultaneous liquid chromatography–mass spectrometry quantification of cefixime and clavulanic acid in human plasma. *J. Chromatogr. Sci.* **2015**, *53*, 694–701. [[CrossRef](#)]
5. Chowdhury, A.M.A.; Uddin, K.N. Analysis of the Occurrence of Antibiotic Resistant Bacteria in the Hospital's Effluent and its Receiving Environment. *Microbiol. Insights* **2022**, *15*, 11786361221078211. [[CrossRef](#)]
6. Shao, S.; Hu, Y.; Cheng, J.; Chen, Y. Research progress on distribution, migration, transformation of antibiotics and antibiotic resistance genes (ARGs) in aquatic environment. *Crit. Rev. Biotechnol.* **2018**, *38*, 1195–1208. [[CrossRef](#)]
7. Turolla, A.; Cattaneo, M.; Marazzi, F.; Mezzanotte, V.; Antonelli, M. Antibiotic resistant bacteria in urban sewage: Role of full-scale wastewater treatment plants on environmental spreading. *Chemosphere* **2018**, *191*, 761–769. [[CrossRef](#)]
8. Ayodele, O.B. Effect of phosphoric acid treatment on kaolinite supported ferrioxalate catalyst for the degradation of amoxicillin in batch photo-Fenton process. *Appl. Clay Sci.* **2013**, *72*, 74–83. [[CrossRef](#)]
9. Acayanka, E.; Tarkwa, J.-B.; Takam, B.; Abia, D.; Serge, N.; Kamgang, G.Y.; Laminsi, S. Removal of various pollutants from wastewater using plasma-modified lignocellulose-derived as a low-cost adsorbent: An overview. *Mini-Rev. Org. Chem.* **2021**, *18*, 434–449. [[CrossRef](#)]
10. Hasanzadeh, V.; Rahmanian, O.; Heidari, M. Cefixime adsorption onto activated carbon prepared by dry thermochemical activation of date fruit residues. *Microchem. J.* **2020**, *152*, 104261. [[CrossRef](#)]
11. Bay, A.; Yazdanbakhsh, A.; Eslami, A.; Rafiee, M. Investigation of sequencing batch moving-bed biofilm reactor to biodegradation of cefixime as emerging pollutant in percent of easily degradable co-substrate. *Int. J. Environ. Anal. Chem.* **2023**, *103*, 2142–2151. [[CrossRef](#)]
12. Hasani, K.; Peyghami, A.; Moharrami, A.; Vosoughi, M.; Dargahi, A. The efficacy of sono-electro-Fenton process for removal of Cefixime antibiotic from aqueous solutions by response surface methodology (RSM) and evaluation of toxicity of effluent by microorganisms. *Arab. J. Chem.* **2020**, *13*, 6122–6139. [[CrossRef](#)]

13. Zouaoui, F.; Bourouina-Bacha, S.; Bourouina, M.; Jaffrezic-Renault, N.; Zine, N.; Errachid, A. Electrochemical sensors based on molecularly imprinted chitosan: A review. *TrAC, Trends Anal. Chem.* **2020**, *130*, 115982. [[CrossRef](#)]
14. Fang, L.; Miao, Y.; Wei, D.; Zhang, Y.; Zhou, Y. Efficient removal of norfloxacin in water using magnetic molecularly imprinted polymer. *Chemosphere* **2021**, *262*, 128032. [[CrossRef](#)]
15. Liao, S.; Zhang, W.; Long, W.; Hou, D.; Yang, X.; Tan, N. Adsorption characteristics, recognition properties, and preliminary application of nordihydroguaiaretic acid molecularly imprinted polymers prepared by sol-gel surface imprinting technology. *Appl. Surf. Sci.* **2016**, *364*, 579–588. [[CrossRef](#)]
16. Arabi, M.; Ostovan, A.; Li, J.; Wang, X.; Zhang, Z.; Choo, J.; Chen, L. Molecular imprinting: Green perspectives and strategies. *Adv. Mater.* **2021**, *33*, 2100543. [[CrossRef](#)]
17. Speltini, A.; Scalabrini, A.; Maraschi, F.; Sturini, M.; Profumo, A. Newest applications of molecularly imprinted polymers for extraction of contaminants from environmental and food matrices: A review. *Anal. Chim. Acta* **2017**, *974*, 1–26. [[CrossRef](#)]
18. Asiabi, H.; Yamini, Y.; Seidi, S.; Ghahramanifard, F. Preparation and evaluation of a novel molecularly imprinted polymer coating for selective extraction of indomethacin from biological samples by electrochemically controlled in-tube solid phase microextraction. *Anal. Chim. Acta* **2016**, *913*, 76–85. [[CrossRef](#)]
19. Pourjavadi, A.; Shakerpoor, A.; Tehrani, Z.M.; Bumajdad, A. Magnetic graphene oxide mesoporous silica hybrid nanoparticles with dendritic pH sensitive moieties coated by PEGylated alginate-co-poly (acrylic acid) for targeted and controlled drug delivery purposes. *J. Polym. Res.* **2015**, *22*, 156. [[CrossRef](#)]
20. Fu, H.; Xu, W.; Wang, H.; Liao, S.; Chen, G. Preparation of magnetic molecularly imprinted polymers for the identification of zearalenone in grains. *Anal. Bioanal. Chem.* **2020**, *412*, 4725–4737. [[CrossRef](#)]
21. Fan, Y.; Zeng, G.; Ma, X. Multi-templates surface molecularly imprinted polymer for rapid separation and analysis of quinolones in water. *Environ. Sci. Pollut. Res.* **2020**, *27*, 7177–7187. [[CrossRef](#)]
22. Huang, S.; Xu, J.; Zheng, J.; Zhu, F.; Xie, L.; Ouyang, G. Synthesis and application of magnetic molecularly imprinted polymers in sample preparation. *Anal. Bioanal. Chem.* **2018**, *410*, 3991–4014. [[CrossRef](#)] [[PubMed](#)]
23. Xu, X.; Chen, S.; Wu, Q. Surface molecular imprinting on polypropylene fibers for rhodamine B selective adsorption. *J. Colloid Interface Sci.* **2012**, *385*, 193–201. [[CrossRef](#)] [[PubMed](#)]
24. Zhang, D.; Tang, J.; Liu, H. Rapid determination of lambda-cyhalothrin using a fluorescent probe based on ionic-liquid-sensitized carbon dots coated with molecularly imprinted polymers. *Anal. Bioanal. Chem.* **2019**, *411*, 5309–5316. [[CrossRef](#)]
25. Gao, B.; Wang, J.; An, F.; Liu, Q. Molecular imprinted material prepared by novel surface imprinting technique for selective adsorption of pirimicarb. *Polymer* **2008**, *49*, 1230–1238. [[CrossRef](#)]
26. Ding, S.; Li, Z.; Cheng, Y.; Du, C.; Gao, J.; Zhang, Y.-W.; Zhang, N.; Li, Z.; Chang, N.; Hu, X. Enhancing adsorption capacity while maintaining specific recognition performance of mesoporous silica: A novel imprinting strategy with amphiphilic ionic liquid as surfactant. *Nanotechnology* **2018**, *29*, 375604. [[CrossRef](#)]
27. Dinc, M.; Esen, C.; Mizaikoff, B. Recent advances on core-shell magnetic molecularly imprinted polymers for biomacromolecules. *TrAC Trends Anal. Chem.* **2019**, *114*, 202–217. [[CrossRef](#)]
28. Chen, N. Application of Magnetic Molecular Imprinted Technology in Fluoroquinolone Antibiotics. In Proceedings of the 2020 5th International Conference on Materials Science, Energy Technology and Environmental Engineering, Shanghai, China, 7–9 August 2020; IOP Conference Series: Earth and Environmental Science. p. 012106.
29. Kryscio, D.R.; Peppas, N.A. Surface imprinted thin polymer film systems with selective recognition for bovine serum albumin. *Anal. Chim. Acta* **2012**, *718*, 109–115. [[CrossRef](#)]
30. Canfarotta, F.; Waters, A.; Sadler, R.; McGill, P.; Guerreiro, A.; Papkovsky, D.; Haupt, K.; Piletsky, S. Biocompatibility and internalization of molecularly imprinted nanoparticles. *Nano Res.* **2016**, *9*, 3463–3477. [[CrossRef](#)]
31. Mirzapour, F.; Sadeghi, M. Magnetic molecular imprinted polymers for in vitro controlled release and solid-phase extraction of dextromethorphan: Synthesize, characterization, and application. *Iran. Polym. J.* **2022**, *31*, 553–571. [[CrossRef](#)]
32. Yan, C.; Zhang, N.; Guan, P.; Chen, P.; Ding, S.; Hou, T.; Hu, X.; Wang, J.; Wang, C. Drug-based magnetic imprinted nanoparticles: Enhanced lysozyme amyloid fibrils cleansing and anti-amyloid fibrils toxicity. *Int. J. Biol. Macromol.* **2020**, *153*, 723–735. [[PubMed](#)]
33. Bhogal, S.; Mohiuddin, I.; Kim, K.-H.; Malik, A.K.; Kaur, K. Restricted access medium magnetic molecularly imprinted polymers: Validation of their suitability as an effective quantitation tool against phthalates in food products packaged in plastic. *Chem. Eng. J.* **2023**, *457*, 141270.
34. Lu, Z.; Zhou, G.; Song, M.; Liu, X.; Tang, H.; Dong, H.; Huo, P.; Yan, F.; Du, P.; Xing, G. Development of magnetic imprinted PEDOT/CdS heterojunction photocatalytic nanoreactors: 3-Dimensional specific recognition for selectively photocatalyzing danofloxacin mesylate. *Appl. Catal. B* **2020**, *268*, 118433.
35. Gaho, M.M.; Memon, G.Z.; Arain, J.B.; Arain, A.J.; Shah, A.; Samejo, M.Q. Synthesis of novel magnetic molecularly imprinted polymers by solid-phase extraction method for removal of norfloxacin. *Chin. J. Anal. Chem* **2022**, *50*, 100079.
36. Li, Z.; Tian, W.; Chu, M.; Zou, M.; Zhao, J. Molecular imprinting functionalization of magnetic biochar to adsorb sulfamethoxazole: Mechanism, regeneration and targeted adsorption. *Process Saf. Environ. Prot.* **2023**, *171*, 238–249.
37. Chang, T.; Liu, Y.; Yan, X.; Liu, S.; Zheng, H. One-pot synthesis of uniform and monodisperse superparamagnetic molecularly imprinted polymer nanospheres through a sol-gel process for selective recognition of bisphenol A in aqueous media. *RSC Adv.* **2016**, *6*, 66297–66306.

38. López, R.; Khan, S.; Torres, S.E.; Wong, A.; Sotomayor, M.D.; Picasso, G. Synthesis and Characterization of Magnetic Molecularly Imprinted Polymer for the Monitoring of Amoxicillin in Real Samples Using the Chromatographic Method. *Magnetochemistry* **2023**, *9*, 92.
39. Li, J.; Zhou, X.; Yan, Y.; Shen, D.; Lu, D.; Guo, Y.; Xie, L.; Deng, B. Selective recognition of gallic acid using hollow magnetic molecularly imprinted polymers with double imprinting surfaces. *Polymers* **2022**, *14*, 175.
40. Hu, C.; Peng, F.; Mi, F.; Wang, Y.; Geng, P.; Pang, L.; Ma, Y.; Li, G.; Li, Y.; Guan, M. SERS-based boronate affinity biosensor with biomimetic specificity and versatility: Surface-imprinted magnetic polymers as recognition elements to detect glycoproteins. *Anal. Chim. Acta* **2022**, *1191*, 339289.
41. Du, L.; Wu, Y.; Zhang, X.; Zhang, F.; Chen, X.; Cheng, Z.; Wu, F.; Tan, K. Preparation of magnetic molecularly imprinted polymers for the rapid and selective separation and enrichment of perfluorooctane sulfonate. *J. Sep. Sci.* **2017**, *40*, 2819–2826.
42. Hemmati, K.; Sahraei, R.; Ghaemy, M. Synthesis and characterization of a novel magnetic molecularly imprinted polymer with incorporated graphene oxide for drug delivery. *Polymer* **2016**, *101*, 257–268. [[CrossRef](#)]
43. Wei, M.; Yan, X.; Liu, S.; Liu, Y. Preparation and evaluation of superparamagnetic core-shell dummy molecularly imprinted polymer for recognition and extraction of organophosphorus pesticide. *J. Mater. Sci.* **2018**, *53*, 4897–4912. [[CrossRef](#)]
44. Muhammad, T.; Cui, L.; Jide, W.; Piletska, E.V.; Guerreiro, A.R.; Piletsky, S.A. Rational design and synthesis of water-compatible molecularly imprinted polymers for selective solid phase extraction of amiodarone. *Anal. Chim. Acta* **2012**, *709*, 98–104. [[PubMed](#)]
45. Niu, M.; Pham-Huy, C.; He, H. Core-shell nanoparticles coated with molecularly imprinted polymers: A review. *Microchim. Acta* **2016**, *183*, 2677–2695.
46. Iskierko, Z.; Sharma, P.S.; Bartold, K.; Pietrzyk-Le, A.; Noworyta, K.; Kutner, W. Molecularly imprinted polymers for separating and sensing of macromolecular compounds and microorganisms. *Biotechnol. Adv.* **2016**, *34*, 30–46.
47. Liu, Z.; Gao, Y.; Jin, L.; Jin, H.; Xu, N.; Yu, X.; Yu, S. Core-shell regeneration magnetic molecularly imprinted polymers-based SERS for sibutramine rapid detection. *ACS Sustain. Chem. Eng.* **2019**, *7*, 8168–8175. [[CrossRef](#)]
48. Duan, Z.-J.; Fan, L.-P.; Fang, G.-Z.; Yi, J.-H.; Wang, S. Novel surface molecularly imprinted sol-gel polymer applied to the online solid phase extraction of methyl-3-quinoxaline-2-carboxylic acid and quinoxaline-2-carboxylic acid from pork muscle. *Anal. Bioanal. Chem.* **2011**, *401*, 2291–2299. [[CrossRef](#)]
49. Aguilar, J.F.; Miranda, J.; Rodriguez, J.; Paez-Hernandez, M.; Ibarra, I. Selective removal of tetracycline residue in milk samples using a molecularly imprinted polymer. *J. Polym. Res.* **2020**, *27*, 176. [[CrossRef](#)]
50. Karrat, A.; Palacios-Santander, J.M.; Amine, A.; Cubillana-Aguilera, L. A novel magnetic molecularly imprinted polymer for selective extraction and determination of quercetin in plant samples. *Anal. Chim. Acta* **2022**, *1203*, 339709. [[CrossRef](#)]
51. Anirudhan, T.; Rejeena, S. Adsorption and hydrolytic activity of trypsin on a carboxylate-functionalized cation exchanger prepared from nanocellulose. *J. Colloid Interface Sci.* **2012**, *381*, 125–136. [[CrossRef](#)]
52. Cáceres, C.; Bravo, C.; Rivas, B.; Moczko, E.; Sáez, P.; García, Y.; Pereira, E. Molecularly imprinted polymers for the selective extraction of bisphenol a and progesterone from aqueous media. *Polymers* **2018**, *10*, 679. [[CrossRef](#)] [[PubMed](#)]

Disclaimer/Publisher's Note: The statements, opinions and data contained in all publications are solely those of the individual author(s) and contributor(s) and not of MDPI and/or the editor(s). MDPI and/or the editor(s) disclaim responsibility for any injury to people or property resulting from any ideas, methods, instructions or products referred to in the content.